European Water 71/72: 27-40, 2020.

Dealing with LSPIV questions on the field: An approach for autonomous flood gauging using UAVs

G. Moraitis* and E. Baltas
Department of Water Resources and Environmental Engineering, School of Civil Engineering, National Technical University of Athens, Heroon Polytechneiou 5, Zografou GR-15780, Greece
* *e-mail: georgemoraitis@central.ntua.gr*

Abstract: In an era when flood phenomena intensify worldwide, the scarcity of proper and systematic flood flow measurements has become a conundrum. As an answer, the non-intrusive Large-Scale Particle Image Velocimetry (LSPIV) method has recently advanced to a contemporary gauging alternative, though several limitations in the field application pose questions. To tackle relevant restrains, this study brings forth a new approach for LSPIV field applications and flood gauging using lightweight unmanned aerial vehicles (UAV). In the core of the suggested approach lies a flexible yet direct and accurate matching technique to define the water surface as reference plane, without the need for fixed Ground Control Points (GCP) on the field. In addition, to address uncertainties relevant to apparatus movements that occur from winds and gusts during field recordings, an error-removing process that utilises digital fictitious GCPs is reported. The proposed techniques, implemented via a purpose-built application, are evaluated under various recording conditions in both laboratory and field studies, with positive results. Overall, the granted autonomy, as a result of the approach, provides applicability of the LSPIV method to practically any section of interest without the need for construction or the presence of personnel in hazardous conditions, allowing for a safe, efficient, and low-cost flood gauging alternative.

Key words: LSPIV; UAV; drone; floods; flood gauging

1. INTRODUCTION

Hydrological monitoring is an exercise of systematic data collection, essential to scientific research and rational water management to, inter alia, determine design criteria, allocate water supplies and deal with extreme events, such as floods. The latter, represent nearly half of the reported weather-related disasters worldwide between 1995 and 2015, affecting 2.3 billion people (UNDRR 2015). Evidently such disasters are directly associated with subsequent, long-term predicament of societal functions (UNDRR 2019), thus, relevant mitigation actions are deemed as a development affair. To address them, consistent, accurate and up-to-date monitoring of hydrometeorological response is required. However, contrary to the information needs and in addition to the often inefficient spatial distribution of existing monitoring networks (Baltas and Mimikou 2009), accessibility and availability of relevant data tend to decline worldwide (Calmant and Seyler 2006; Dai et al. 2009; Sichangi et al. 2016). The need for vigilance and suitable hydrometeorological data of proper scale (Feloni et al. 2018; Hamilton 2012; Kossieris et al. 2018) are becoming urgently important, as flood phenomena shift towards hazardous, acute flash floods.

Operational monitoring of streamflow is commonly conducted by interpreting the stage gauge measurements through section-specific rating curves. Though permanent stream gauges are constructed to provide continuous measurements, they often fail to provide the crucial information of flood peak discharge due to overtopping, lack of granularity, etc. (Borga et al. 2008; WMO 2008). Furthermore, rating curves are susceptible to various sources of uncertainty, including those streaming from calibration and extrapolation processes (Di Baldassarre and Montanari 2009; Götzinger and Bárdossy 2008; Petersen-Øverleir 2006). For the latter, paucity of stage-discharge measurements for extreme events limits the confidence in their applicability, albeit calibrated for a wide range of flows. Extreme flood events require timely in situ measurements in priority sections

to acquire the desired information. Though merits are not to be ignored, apart from the known limitations of tracer dilution method (e.g. Capesius et al., 2005; Sappa et al., 2015) and the sensitivity of equipment used for velocity area method (e.g. Dombroski and Crimaldi, 2007; Mueller and Wagner, 2009; Voulgaris and Trowbridge, 1998) the safety concerns from the exposure of personnel to hazardous conditions are not to be neglected. High velocities, acute rate changes, debris, and often inaccessible sites, greatly limit the applicability of conventional methods during extreme events.

However, alternative methods may implement non-invasive remote sensing, such as techniques for extracting hydrological information from satellite imagery (see for example Bjerklie et al., 2003; Calmant and Seyler, 2006; Sichangi et al., 2016). Despite a significant progress in this field, the need for event-based in situ measurements during extreme events remains, in pursuance of proper data for the model's calibration and validation processes. Moreover, satellite observations currently lack the spatial and temporal granularity to capture the hydrological response of mountainous and/or small catchments and intermittent rivers.

A promising nonintrusive approach, suitable for rapidly varying flows, is that of Large-Scale Particle Image Velocimetry (LSPIV). Deriving from the laboratory technique of Particle Image Velocimetry (PIV) (Willert and Gharib 1991), LSPIV is a visual method that gauges the surface distribution of the instantaneous velocity fields through successive recordings. Unlike satellite imagery, the field-scaled recordings of LSPIV are adjusted to better address site-specific needs and limitations (e.g. small channel widths, obstacles in the field of view (FoV), extreme luminosity or shading etc.). Moreover, contemporary image capturing equipment, including inexpensive commercial solutions, are capable of high resolution and density recordings. As a result, LSPIV offers the required spatial and temporal granularity to gauge flood events.

LSPIV has been successfully implemented in scaled experiments of e.g. bridge abutments (Morales et al. 2008), hydropower plants (Cesare et al. 2009), lake water circulation patterns (Admiraal et al. 2004) and shallow flows (Muste et al. 2014). Nevertheless, LSPIV has been proven efficient beyond laboratory conditions as well. Indicative of the method's capabilities are the field studies over wide ranges of discharge (Creutin et al. 2003; Jodeau et al. 2008) and during flood events (Le Coz et al. 2010; Tauro et al. 2016a). In addition, measurements that were conducted using hovering UAVs (Bolognesi et al. 2017; Detert and Weitbrecht 2015; Moraitis and Baltas 2019; Tauro et al. 2016b) showcase their feasibility as recording apparatus. However, the LSPIV method may be further enhanced as a flood gauging alternative by removing constrains associated with required site constructions or infrastructures and the accessibility of the site during extreme events.

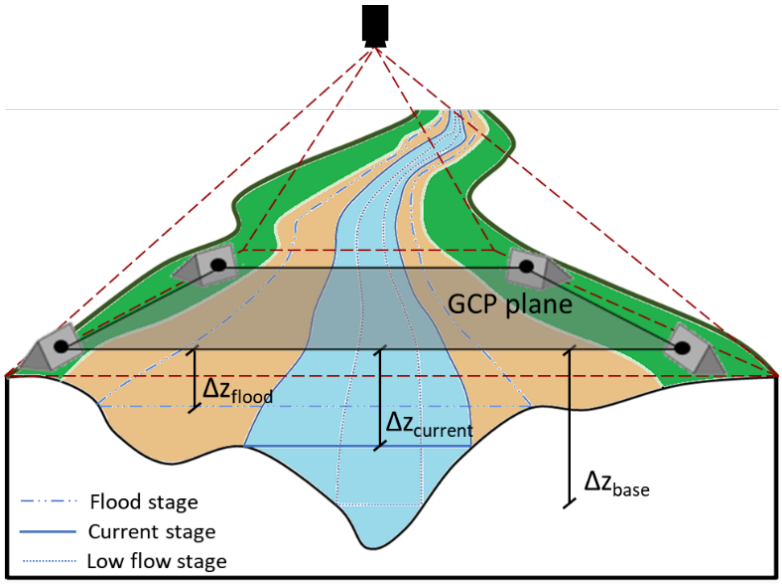

Figure 1. Vertical error of GCP reference plane to actual water level surfaces

Whilst autonomy of the method is desired, both ground-based and fixed-position airborne camera recordings make use of Ground Control Points (GCPs) to infer digital information to a real-world coordinate system, as in *Figure 1* above. Considering that LSPIV investigates surface velocity fields by means of object movement size, the projection of the digital displacement should be constantly referenced to the water surface plane. Typically, GCPs are placed or marked by hand on attainable spots, above the current and the potential flood water levels to ensure they remain detectable. Fixed GCPs in each section, besides maintenance and cost issues, inherently lack the ability to steadily refer to the dynamically varying water surface level, as illustrated in Figure 1. As a result, deviations from the surface plane generate errors (Creutin et al. 2003; Jodeau et al. 2008) that affect both accuracy and consistency of the final measurements.

Additional errors to the measurements are induced while inferring the real-world size of a pixel, that is the vertical and horizontal size in e.g. meters for the image pixel, based on either the distances between off-plane GCPs or as raw analogy based on the camera and water surface distance. Applicability of the latter though is confined, as it requires knowledge of the actual water level, an information that is practically requested during hydrometric gauging. Thus, the use of a single, constant pixel-to-world size grid leads to sizing errors when mapping LSPIV object displacements to real world coordinates (see Figure 2) and reduces the accuracy of final results.

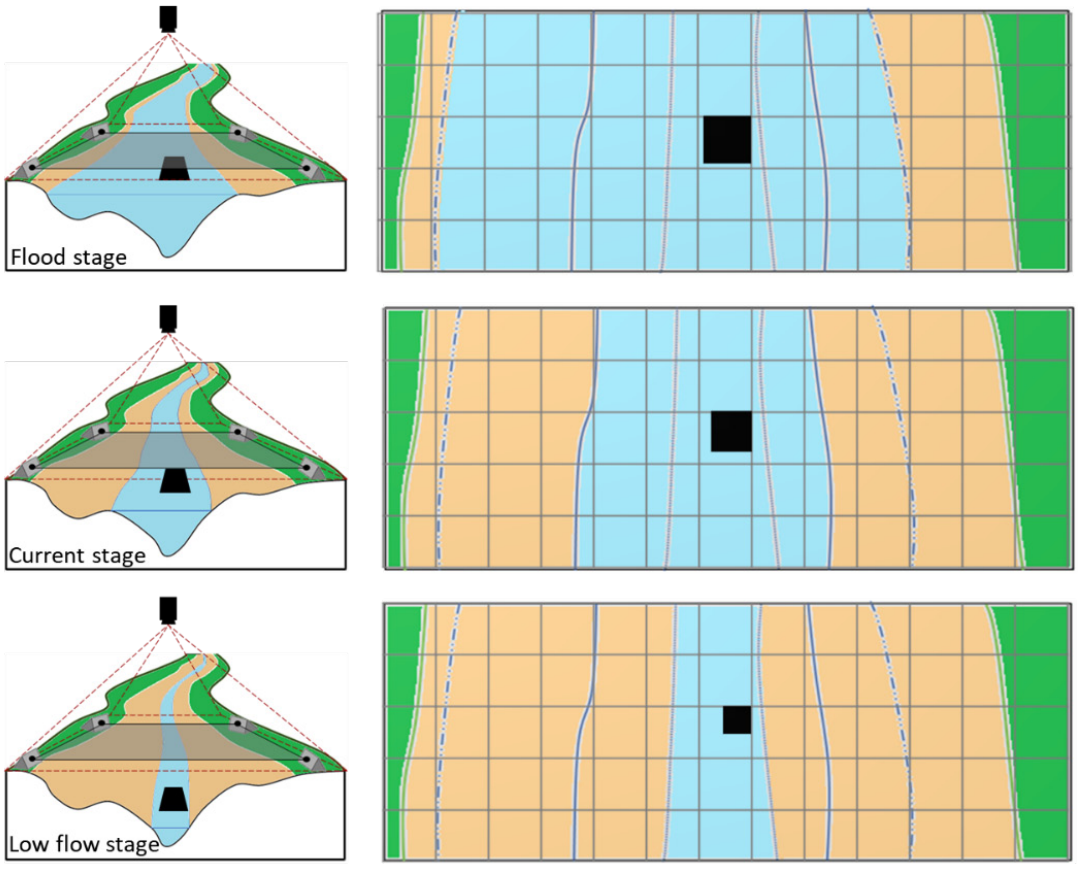

Figure 2. Rectangular floating object projection and sizing (steady pixel-to-world transformation grid) using the GCP reference plane, for 3 distinct flowing conditions

UAV based studies also report the significance of camera stability during hovering to the final results (Detert and Weitbrecht 2015; Tauro et al. 2016b). Gimbal stabilization mechanisms can absorb the usual aircraft vibrations and minor movements or rotations. However, flight conditions are rarely optimal, particularly during flood generating weather events. With multiple degrees of freedom for UAV-based recordings, increased wind speeds and unexpected gusts during flight may induce significant relevant movement errors to the final data.

In this context, our study seeks to enhance LSPIV field applicability by disconnecting it from

conventional GCPs and attaining projection and camera motion errors of UAV based recordings. Thus, moving drone recordings could be conducted to allow for continuous scanning of larger water bodies. The proposed approach utilizes floating objects to specify the water surface as the LSPIV plane of measurement and obtain an accurate estimation of the pixel size to real world coordinates. A purpose-built code is developed to deploy the process. To evaluate the performance and identify pros and cons for the approach, application studies were conducted under both laboratory and field conditions.

2. A GCP-INDEPENDENT LSPIV APPROACH

Transformation from the pixel coordinates of the recordings to real world coordinates lays in the core of LSPIV applications. Inverse mapping of information from the 2D coordinates of the image plane back to real world dimensions requires knowledge of relevant transformation parameters, otherwise it is completed through simplifications or assumptions. Methods that infer the pixel-to-world analogy based on the real and pixel-wise distance of GCPs, though easier to apply, lead to estimation errors mainly due to improper plane reference. The magnitude of such errors depends on the vertical deviation of the reference level to the water surface. To address this source of uncertainty, the acquisition of transformation parameters through camera resectioning process is proposed.

Camera resectioning, also known as camera calibration, is the process of estimating the camera parameters that define the relationship of an image recording to the real world. Defining the [x,y] 2D pixel coordinate system on the non-skewed ($\gamma = 0$) image plane and the arbitrary [X,Y,Z] 3D real world system coordinates, the transformation through the pinhole camera model is described based on the following equations:

$$x = \frac{1}{s_x} \cdot f \cdot \frac{R_{11}X+R_{12}Y+R_{13}Z+T_X}{R_{31}X+R_{32}Y+R_{33}Z+T_Z} + x_0 \quad (1)$$

$$y = \frac{1}{s_y} \cdot f \cdot \frac{R_{21}X+R_{22}Y+R_{23}Z+T_Y}{R_{31}X+R_{32}Y+R_{33}Z+T_Z} + y_0 \quad (2)$$

where f the focal length, s_x and s_y the horizontal and vertical effective size of pixels respectively (in mm) and x_0, y_0 the principal point coordinates, which compose the intrinsic camera parameters. The latter, remain constant regardless of the camera position that is described by rotations $R_{i,j}$ and translation T in respect to the scene plane (extrinsic parameters). For the pinhole camera model assumption to be valid, lens distortions must be removed to create an ideal rectilinear image plane. To acquire the intrinsic and extrinsic parameters that define the transformation, camera calibration requires points of known coordinates in the real-world system for each scene plane.

For the LSPIV applications though, the water surface is the motion field of interest on which velocity estimations are referenced. Thus, the water surface may be assumed as the single scene plane on which all points of interest reside. In order to make proper reference and match the two planes, the camera calibration points must actually reside on the water surface. To achieve this, we propose the use of floating objects of known dimensions which allows the transfer of GCP to points coplanar with any particle measured on the free surface by LSPIV. Based on a floating calibration target of known dimensions, coplanar to the surface and after removing radial distortions, the Zhang camera calibration (Zhang 2000) is utilized, which requires no knowledge of motion for the calibration target.

Based on this technique, the pixel-to-world analogy required for the backward projection transformation of LSPIV measurements is constantly revised to account for different water surfaces and/or different camera positions, as in *Figure 3*. The latter is a useful capability during field recordings with UAV, as it allows personnel to readjust and optimize the recording position at any

time, e.g. to address illumination or shading restrains that may occur. Note that the proposed workflow supports both tilted and moving camera recordings, increasing the flexibility and applicability of the technique.

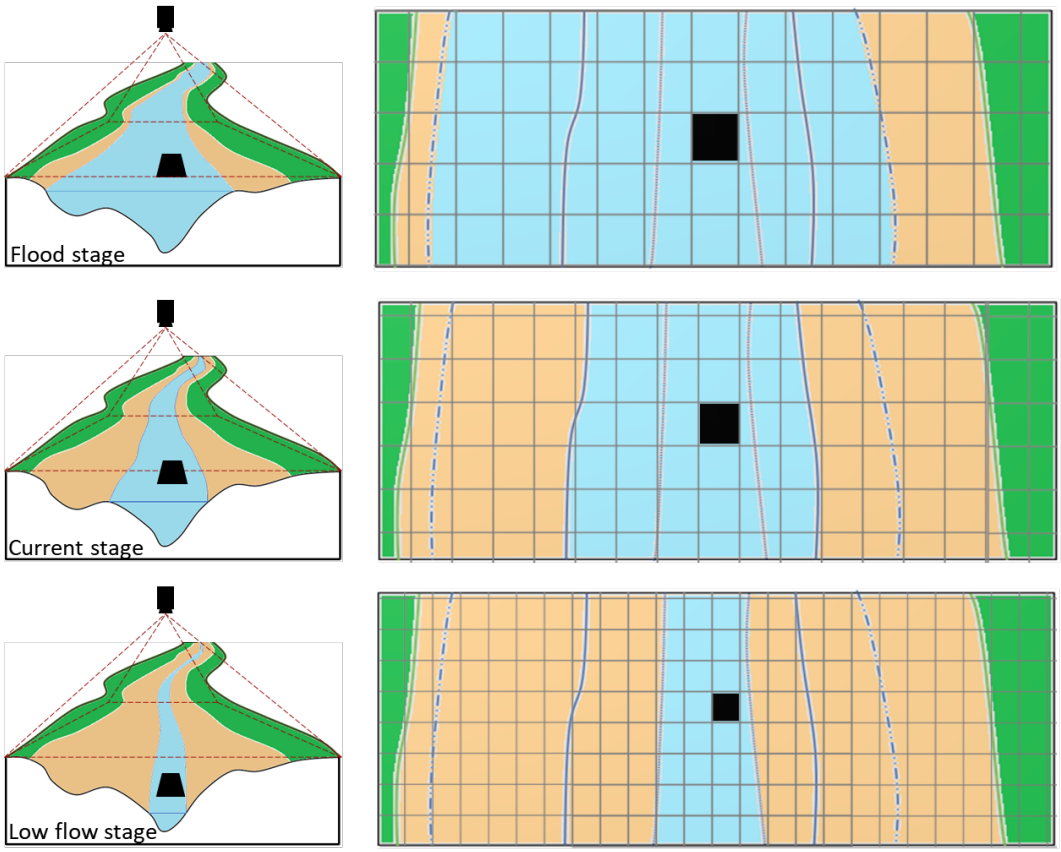

Figure 3. Rectangular floating object projection and sizing (adjustable pixel-to-world transformation grid) using the proposed technique, for 3 distinct flowing conditions

In field conditions however, the accuracy of the UAV-based approach is often challenged, as wind gusts continuously relocate the apparatus and create an ever-moving recording system. In that system both the size and the direction of motion are not fixed, but present a rather random and dynamic profile. Such motions translate, rotate, re-size and skew the recorded scenes, as pictured in *Figure 4* below, creating relevant movement between images even for fixed points.

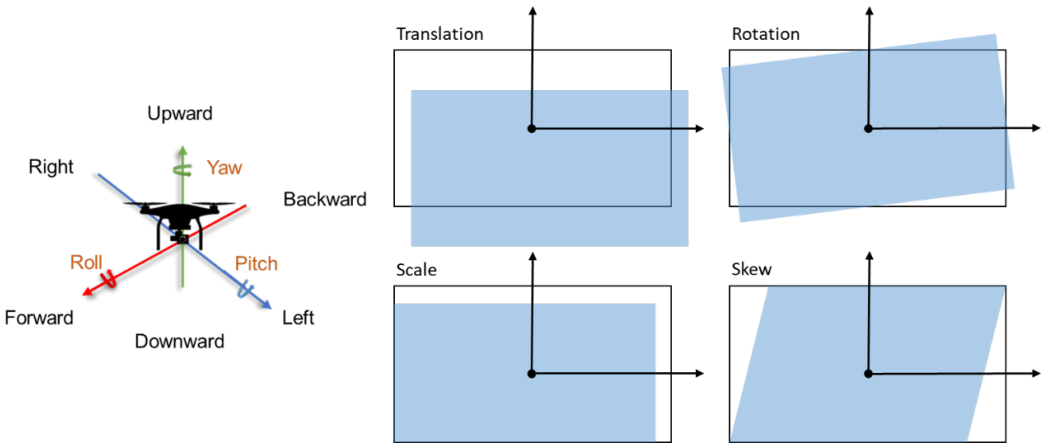

Figure 4. UAV movement and rotation degrees of freedom (left) and scene errors from camera motions (right)

To remove false motion vectors and rectify scene deviations from any frame A to a later

recorded frame B, this work proposes the implementation of inverse geometric transformation, with properly calibrated parameters, based on keypoints of known coordinates, common between scenes. This process, known as feature-based image registration, is deployed in 3 fundamental steps: a) extract feature keypoints in intensity images using a feature detector, b) identify matching feature pairs and their correspondence between images based on binary descriptors and c) calibrate the transformation parameters that best fit the motion vectors between images, after excluding outliers. Since the unintentional movements of the recording system are unpredictable, effects from a composite motion spectrum should be considered, leading to the suggestion of affine transformation, as it accounts for all possible displacement effects of translations ($\Delta x, \Delta y$), rotations (θ_x, θ_y), dilations (s_x, s_y) and shears (ε) of the 2D image plane (Fuh and Maragos 1991). Those affine transformation parameters need to be calibrated for each LSPIV image pair, based on the motion displacement of steady points of known coordinates and their correspondence for the given pair. For this matter, as this study intends to provide a GCP-independent approach, the detection and use of suitable, temporary digital GCPs is proposed. Those distinctive points are sought in the image space and tracked between successive recordings. Considering that the water surface is the field that inherently contains motion, the digital GCPs must reside only outside that part of the image. This allows to properly fit transformation parameters and capture the relevant movement/deformation of the scene due to camera relocation, without influence from the actual water movement, as seen in Figure 5. Though water surface points are not included in the transformation calibration, the transformation per se is applied to them as well, to correct the relevant movement errors on the surface velocity vectors caused by the camera motions.

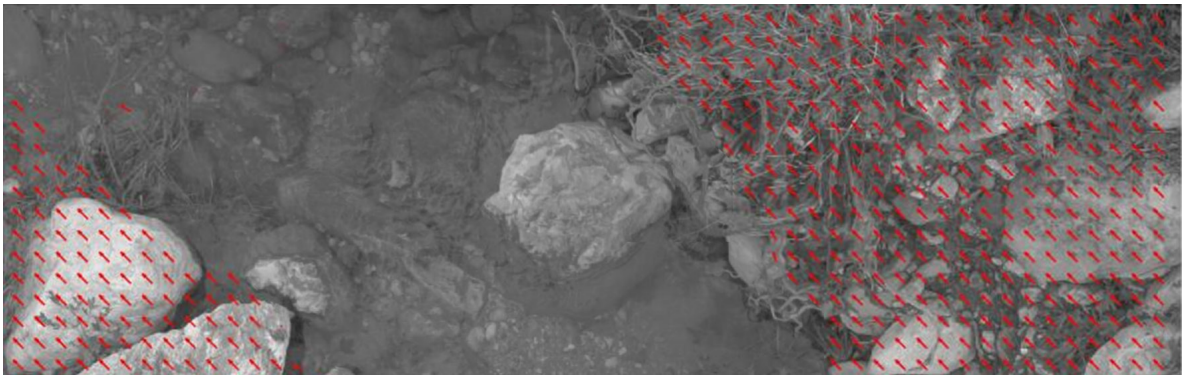

Figure 5. Snapshot of relevant movement error vectors for a field study image pair

In the first step, the image pairs are transformed into intensity images (gray scale) and corner point objects of high contrast are detected in each, using the Features from Accelerated Segment Test (FAST) feature detector of Rosten and Drummond (2005). Each corner point is identified based on the higher or lower intensity value of its adjacent pixels in a 16-pixel radius circle. After creating a large number of random corner objects in each image, keypoint descriptors are assigned to all points using the Fast Retina Key-point (FREAK) methodology (Alahi et al. 2012). The latter, produces a set of descriptors in the form of a binary string by comparing, post-Gaussian smoothing, intensity values between uncorrelated point pairs under a sampling pattern, to capture and label the relationship of each point to its surrounding in a scale and rotation-invariant manner (Hassaballah et al. 2019). The FREAK descriptors methodology is suggested in this work, as it introduces lower memory load to the process and reduces computational time. Subsequently, descriptors of each keypoint are used in a nearest neighbor search to detect the strongest, unique matches and their correspondence in each image pair. Through this feature matching process, the new position of the objects in the next scene and the relevant motion vectors can be retrieved. To ensure better spatial distribution of the final corner points throughout the image, it is recommended to segment the images into at least 4 regions of interest (ROI) to which the previous steps are applied. Thus, the final point-set consists of the strongest matches for each image region, and creates a better spatial

distribution for the calibration set. Using those points as temporal, digital GCPs, the proposed methodology suggests the use of least squares fitting principal in conjunction with an outlier detection algorithm (Fischler and Bolles 1981; Torr 2002) to define the transformation that gives the best similarity. The calibrated affine transformation is then applied at the 2D image coordinates system [x,y], translating the relevant position of scene objects from frame B to frame A coordinates and removing nonexistent movement.

In summary, the above presented methodological approach aims to offer independence of LSPIV field applications from fixed GCP and a continuous reference to the actual surface velocity field level, while also addressing uncertainty of final data from camera motion. To assess the performance of the suggested process a series of laboratory and field studies were undertaken and are presented in the next paragraphs.

3. PRELIMINARY LABORATORY STUDY

The experimental study took place in the Laboratory of Applied Hydraulics of the NTUA Campus, equipped with a 200 L/s capacity recirculating supply system. The laboratory apparatus used were a flume and a Pitot tube for point velocity measurements, seen in *Figure 6* . The flume is 11 meters in length and has a constant rectangular cross section (25.5 cm x 50 cm).

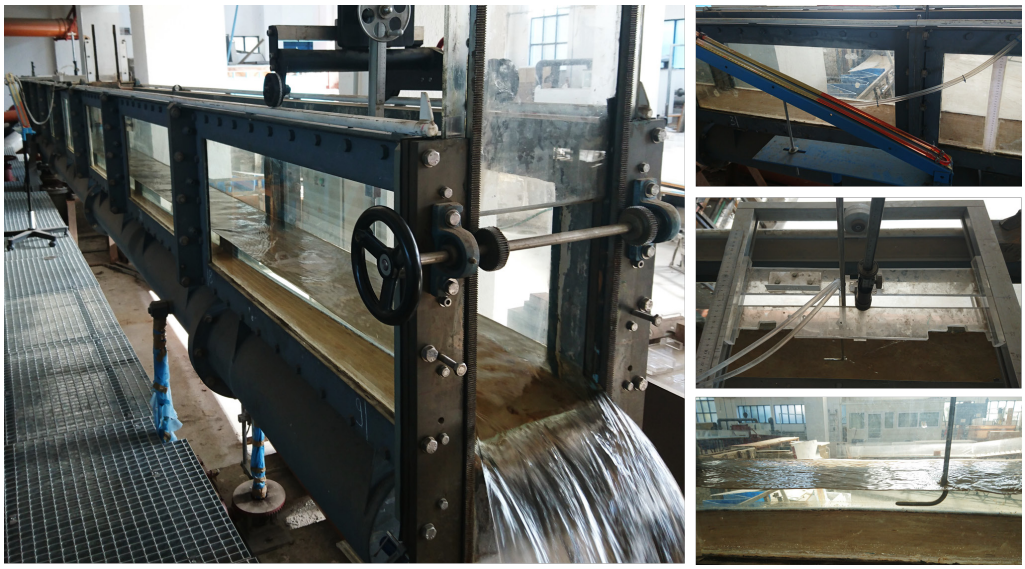

Figure 6. The 11-meter flume (left) and the calibrated Pitot tube (right) used for the study

For this study, 4 Full-HD recording configurations were examined, differing in terms of water velocities and recording height. For each configuration a subset of 3 calibration target sizes (4 cm, 5 cm, 6 cm) and 2 frame rates (30 fps and 60 fps) are defined, composing a set of 24 scenario configurations investigated, listed in *Table 1*. Inhouse laboratory lights kept illumination conditions constant throughout the experiment. Velocity measurements for each configuration were made at the same cross section and the velocity dip phenomenon was considered. Laminar flow is achieved within the first 4.5 meters of the flume, thus, velocities measured with the Pitot tube were considered stable.

Detailed presentation and comparison between each examined scenario configuration would be impractical, therefor, laboratory results are grouped and presented. The first clustering of laboratory measurements is done according to the size of the calibration object (4, 5 and 6 cm) and presented in *Figure 7*. Density plots and inner placed boxplots, known as violin plots, are used to indicate the distribution and statistical characteristics of the measurements' error.

Table 1. Parameters for the 24 scenario configurations of the laboratory study

Recording parameters	Scenario configuration ID											
	#1	#2	#3	#4	#5	#6	#7	#8	#9	#10	#11	#12
Recording height (m)	0.95	0.95	0.95	0.95	0.95	0.95	1.01	1.01	1.01	1.01	1.01	1.01
Reference velocity (m/s)	0.28	0.28	0.28	0.28	0.28	0.28	0.26	0.26	0.26	0.26	0.26	0.26
Calibration target size (cm)	4	4	5	5	6	6	4	4	5	5	6	6
Frame rate (fps)	30	60	30	60	30	60	30	60	30	60	30	60

Recording parameters	Scenario configuration ID											
	#13	#14	#15	#16	#17	#18	#19	#20	#21	#22	#23	#24
Recording height (m)	1.04	1.04	1.04	1.04	1.04	1.04	1.32	1.32	1.32	1.32	1.32	1.32
Reference velocity (m/s)	0.22	0.22	0.22	0.22	0.22	0.22	0.22	0.22	0.22	0.22	0.22	0.22
Calibration target size (cm)	4	4	5	5	6	6	4	4	5	5	6	6
Frame rate (fps)	30	60	30	60	30	60	30	60	30	60	30	60

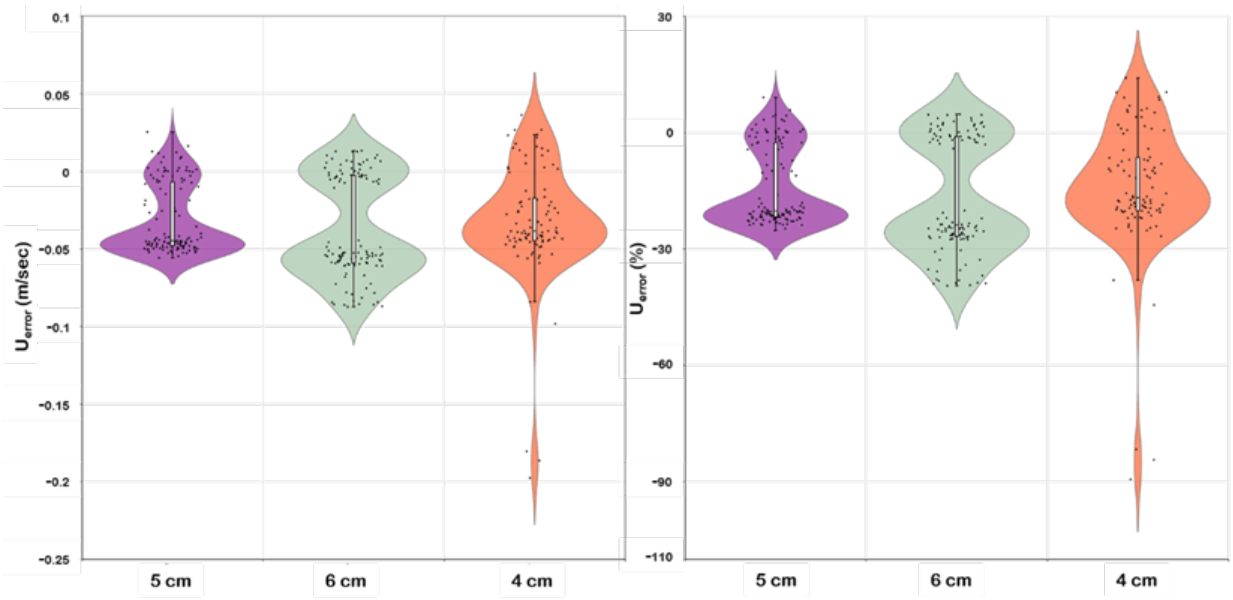

Figure 7. Absolute (left) and percent (right) velocity measurement errors based on calibration target size

Velocity measurements based on the recorded object size are uniformed, with similar statistical characteristics, excluding the outliers for the smallest object measurements. Median of absolute velocity errors is near -0.05m/sec and lower. Regarding the precession of measurements, two subsets of velocity estimations can be visually identified in the violin plots of *Figure 7*. The first cluster has error values near 0, while the second consists of estimations with errors around -0.05 m/sec.

Examination of laboratory measurements based on the 2 recording rates indicated no major effect to the velocity estimation errors. The next measurement categorization and examination is based on the recording configuration as presented in *Table 2*.

Table 2. Scenario configuration groups based on reference velocity and recording height

	Scenario A	Scenario B	Scenario C	Scenario D
Recording height (m)	0.95	1.01	1.04	1.32
Reference velocity (m/s)	0.28	0.26	0.22	0.22

Velocity errors are presented in both absolute and percentage form in *Figure 8*. Median for the higher velocity configurations revolves around 0, with maximum 10% interquartile ranges, while

lower velocity and recording from greater height underestimate the surface velocity. Small interquartile ranges and clustering of measurements, depicted by the lateral expansion of the density plot, indicate consistent behavior in measurements. Clustering of individual measurements that was previously noticed within the violin plot is now obvious between scenario configurations. Scenario results differ between the configuration duets A-B and C-D, with a downward shift of nearly 0.05 m/sec.

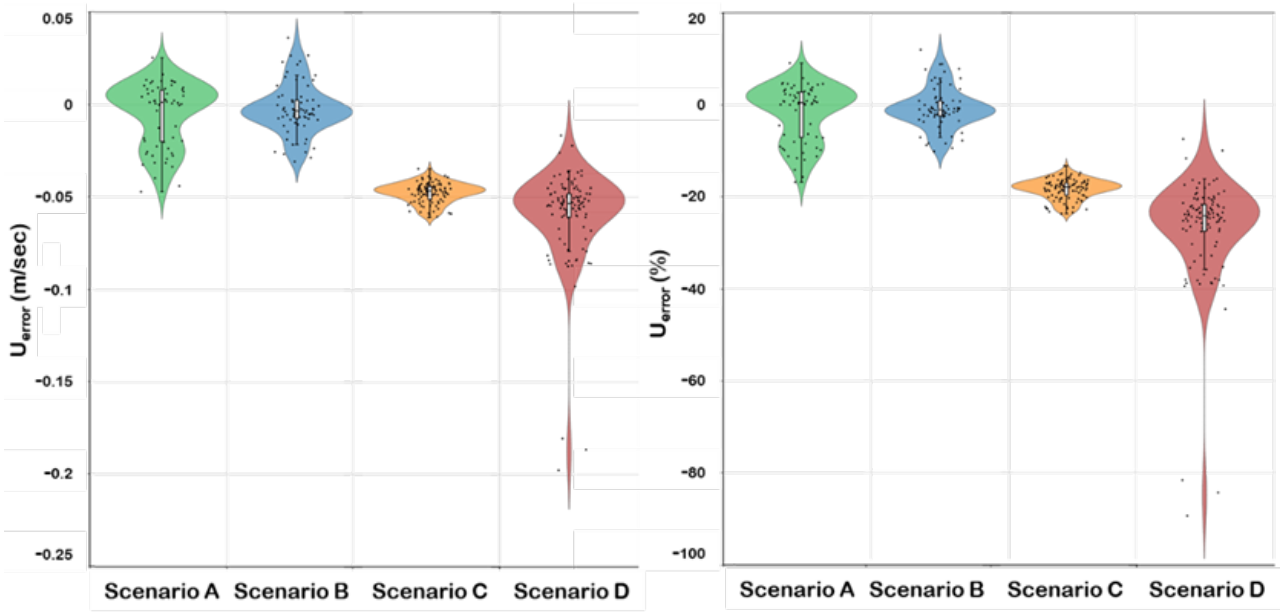

Figure 8. Absolute (left) and percent (right) velocity measurement errors for the 4 scenario configurations

Examination of results based on the 2 Pitot-tube calibrations that took place during the laboratory study is presented in Figure 9. The boxplots for absolute error and the ratio of measured ($U_{measured}$) to reference velocity ($U_{reference}$) are plotted for the 2 subsets of laboratory data based on calibration.

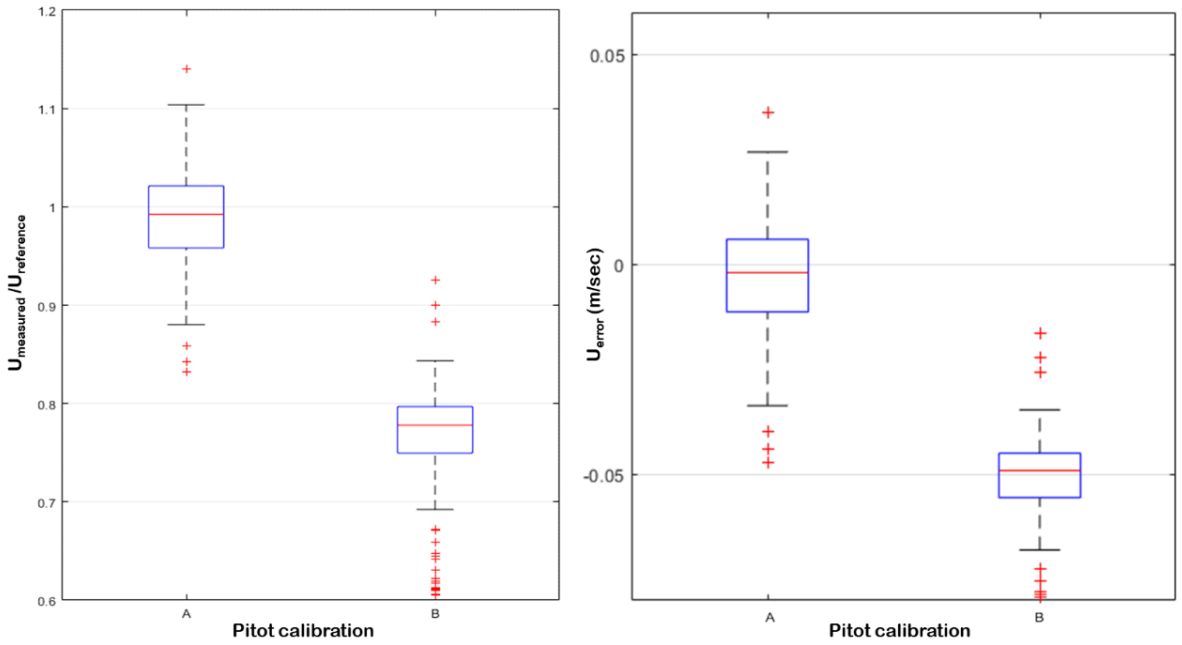

Figure 9. $U_{measured}/U_{reference}$ ratio (left) and absolute error (right) (m/sec) for measurements grouped based on the 2 Pitot calibrations in the laboratory study

Corresponding to the velocity error found for scenarios configurations C and D, underestimation of velocities occurs for the second set of laboratory data, following calibration B of the Pitot tube. Despite the bias induced possibly by calibration errors, laboratory measurements demonstrate similar statistical characteristics with ± 0.03 m/sec absolute error range and ±15% precision.

4. FIELD APPLICATION

To assess field applicability of the proposed LSPIV approach, 2 studies were conducted within a flood prone basin. The Rafina basin, subjected to an intense urbanization in the latest years (Kochilakis et al. 2016), is located in Eastern Attica, Greece and spans over 123 km^2. The first study area (section A) is located near a stream junction in Drafi, with mainly gravel streambed and considerable bank vegetation and trees alongside. As a result, dense shadows and lighting variations create challenging recording conditions in section A. The second study area (section B) is located 800 meters upstream of the outfall in Rafina Gulf with considerable bank vegetation. Lighting conditions for recordings are not challenging due to wider channel section and less trees along the course. In both sites, low flow of 15.98 l/sec and 96.48 l/sec respectively was measured in the main channel thalweg.

Figure 10. Satellite images of section A & B upstream of the Rafina Gulf (Images from Google Earth)

Table 3. Depth and velocity measurements for section A and section B

Section A		
Vertical distance from 1st point (m)	Depth measurement (m)	Velocity (m/s)
0.00	0.02	0.05
0.10	0.08	0.20
0.20	0.21	0.24
0.30	0.22	0.25
0.40	0.22	0.25
0.50	0.05	0.23

Section B		
Vertical distance from 1st point (m)	Depth measurement (m)	Velocity (m/s)
0.00	0.12	0.05
0.25	0.16	0.23
0.50	0.23	0.95
0.75	0.19	0.52
1.00	0.15	0.28
1.15	0.10	0.10
1.30	0.08	0.05

Velocity measurements were obtained with the use of a current meter, properly calibrated for low velocities. The velocities and depths for each section are found in Table 3. Recording apparatus consisted of a commercial drone (DJI Phantom 4), equipped with a camera capable of recording FullHD videos with up to 120 fps and an integrated gimbal, used for a range of recording altitudes in each section. According to a near-by meteorological station, during field studies in both sites, sunlight was obscured as skies were mostly clouded (~80% coverage), while wind speeds of up to 38 km/hr (10.55 m/s) are reported, with North/North-West direction. No precipitation event occurred during the recordings.

As in the laboratory study, recording variations were examined. Field velocity measurements derived from both hovering and moving drone recordings, to evaluate the overall performance of the two-dimensional dynamic calibration and the elimination of relevant movement errors using digital GCPs in field conditions. To better reproduce non-ideal field conditions, both motion (vertical, horizontal and/or lateral) and rotational random errors were manually induced during field recordings.

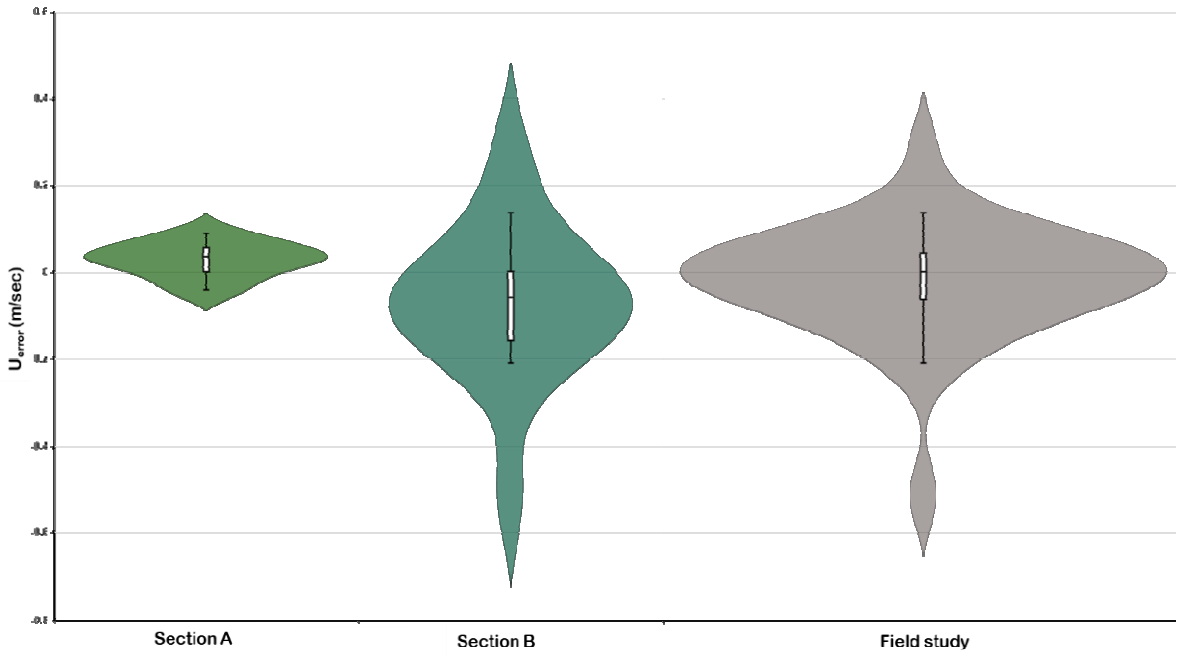

Figure 11. Velocity estimation errors in section A, section B and in combination

Figure 11 illustrates the overall performance of the field application both per study area and in combination. Violin plots and inner boxplots indicate the error distribution characteristics. In comparison to the laboratory measurements, field measurements maintain a uniform behaviour despite the different recording conditions, velocity ranges and random errors of each field study. No obvious bias or recording clustering is depicted.

Although lighting conditions were not optimum, velocity measurements in section A performed consistently, with errors similar to those of the laboratory (<0.1 m/sec) and ± 0.048 m/sec RMSE. Evaluation of total measurements of section A translate in 14.7% mean absolute error. For the study area near the outfalls, section B, higher velocities and velocity ranges are present in the stream flow. RMSE for measurements of section B in total is ± 0.19 m/sec, while average magnitude of velocity errors remains similar, at 14.87% for section B estimations.

The two field studies were designed so that, in combination, they represent a wide range of field conditions, including different flow velocities, streambeds, lighting and recording conditions. As mentioned, field studies performed similarly with identical errors. In this context, merging measurements as one field study and evaluating results in total, could provide a general view of the application for a variety of field parameters. Thus, in total, the field application RMSE is ±0.097 m/sec with 0 m/sec median, showcasing no obvious bias in measurements with the proposed

approach. Indicative of the field application performance is the single rise in the density plot of Figure 11 with no sub-clustering or large sets of residuals. In addition, field velocity errors are ±14.77%, indicating that performance remained practically identical outside laboratory conditions, despite the non-ideal field and meteorological conditions.

At this point, it is worth mentioning, that the UAV based PIV field applications of Bolognesi et al. (2017), with the use of real, riparian GCPs and similar flow velocities (0.034-0.27m/s) report differences that vary from 8.1% up to 26.5% against reference velocities obtained using total stations. In the same work, removal of the GCPs further increased the error by more than 6%. Also, in the work presented by Tauro et al. (2016b) for higher flow velocities, the airborne LSPIV estimations underestimate the mean maximum velocity by up to 13.84% against current meter measurements.

5. CONCLUSIONS AND FUTURE RESEARCH

This study presents an approach on flood gauging using UAVs and dealing with known limitations of LSPIV application on the field by disconnecting it from GCPs and removing camera motion errors of any size. The work shows that accurate reference to any water surface field is attainable, while in conjunction with the use of UAVs, it allows the implementation of LSPIV measurements to practically any stream. In addition to facilitate the application of LSPIV in multiple sites, a process to remove miscellaneous camera movement errors is reported. This process utilizes temporal digital GCPs and descriptors to detect, size and subsequently remove relevant movement errors. Such errors can be induced either circumstantially by strong winds and gusts or through UAV maneuvers to optimize the recording position. The suggested process, deployable through a purpose-built code, is evaluated through a sum of laboratory and field applications. Through the implementation, a steady performance profile is demonstrated for various recording configurations under both laboratory and field conditions. Surface field velocity was estimated with ±15% precision for laboratory measurements and ±14.77% under field conditions with a moving UAV, indicating that the effects from both the non-ideal field and meteorological conditions, and the externally induced motion errors to the recording system were efficiently resolved. With stable and valid performance tested under non-optimal conditions, the method presented in this paper proves to be a reliable alternative for flood gauging applications. As the goal of implementing the proposed LSPIV approach is to acquire flow discharge data, attention should also be paid in the transformation of surface velocity to discharge. Implementation of entropy probability density function methods are proposed (see for example Chao-Lin and Abidin 1995; Chiu 1988; Farina et al. 2014; Moramarco et al. 2017) to establish the relationship between the surface velocity and the mean velocity and estimate the flow discharge in the section. Overall, the proposed approach is useful for flood gauging at multiple sections of interest with no constructions or personnel presence needed, thus making safe and low-cost measurements possible in both gauged and ungauged basins. Resulting measurements could be leveraged, inter alia, to explore hydrological characteristics of a basin and to address uncertainties, such as rating curve extrapolation uncertainties, which are likely to affect the flood resilience strategy of a region. Whilst analysis of the latter is essential, future research and applications should also investigate technical improvements by exploring the use of artificial calibration targets, e.g. with the use of laser projected calibration targets or AI techniques, in addition to alternative recording apparatus, like infrared camera or even smartphone cameras to supply crowd-sourced runoff data. To better assess the merits and limitations, this work should be scaled into a pilot monitoring network and tested for both normal and extreme flow conditions.

AKNWOLEDGEMENTS

We are immensely grateful to Andreas Athanasopoulos for generously providing us the drone and performing all necessary recording configurations. We are also grateful to Nikolaos Dervos for

assisting us throughout the field studies in Rafina basin and especially for carrying out the current meter calibrations and measurements. Special thanks to Yiannis Patselis for assisting and the Laboratory of Applied Hydraulics of the NTUA Campus for authorizing the preliminary experimental investigation. This work stems from the MSc thesis of G. Moraitis, under the supervision of Prof. E. Baltas. An initial version of the paper has been presented in the 14th Conference of the HHA, Volos, Greece, 16 – 17 May 2019.

REFERENCES

Admiraal, D. M., Stansbury, J. S., and Haberman, C. J. (2004). "Case Study: Particle Velocimetry in a Model of Lake Ogallala." Journal of Hydraulic Engineering, 130(7), 599–607.

Alahi, A., Ortiz, R., and Vandergheynst, P. (2012). "FREAK: Fast Retina Keypoint." 2012 IEEE Conference on Computer Vision and Pattern Recognition, IEEE, 510–517.

Di Baldassarre, G., and Montanari, A. (2009). "Uncertainty in river discharge observations: A quantitative analysis." Hydrology and Earth System Sciences, 13(6), 913–921.

Baltas, E. A., and Mimikou, M. A. (2009). "GIS-based optimisation of the hydrometeorological network in Greece." International Journal of Digital Earth, 2(2), 171–185.

Bjerklie, D. M., Dingman, S. L., Vorosmarty, C. J., Bolster, C. H., and Congalton, R. G. (2003). "Evaluating the potential for measuring river discharge from space." Journal of Hydrology, 278(1–4), 17–38.

Bolognesi, M., Farina, G., Alvisi, S., Franchini, M., Pellegrinelli, A., and Russo, P. (2017). "Measurement of surface velocity in open channels using a lightweight remotely piloted aircraft system." Geomatics, Natural Hazards and Risk, Taylor & Francis, 8(1), 73–86.

Borga, M., Gaume, E., Creutin, J. D., and Marchi, L. (2008). "Surveying flash floods: gauging the ungauged extremes." Hydrological Processes, 22(18), 3883–3885.

Calmant, S., and Seyler, F. (2006). "Continental surface waters from satellite altimetry." Comptes Rendus - Geoscience, 338(14–15), 1113–1122.

Capesius, J. P., Sullivan, J. R., O'Neill, G. B., and Williams, C. A. (2005). Using the tracer-dilution discharge method to develop streamflow records for ice-affected streams in Colorado. Scientific Investigations Report.

Cesare, G. De, Ribeiro, J. M., Kantoush, S. A., and Matteo, P. E. A. (2009). "River intake and desander efficiency testing on a physical model using UVP and LSPIV." (2007), 47–50.

Chao-Lin, C., and Abidin, S. C. A. (1995). "Maximum and Mean Velocities and Entropy in Open-Channel Flow." Journal of Hydraulic Engineering, American Society of Civil Engineers, 121(1), 26–35.

Chiu, C. (1988). "Entropy and 2-D Velocity Distribution in Open Channels." Journal of Hydraulic Engineering, 114(7), 738–756.

Le Coz, J., Hauet, A., Pierrefeu, G., Dramais, G., and Camenen, B. (2010). "Performance of image-based velocimetry (LSPIV) applied to flash-flood discharge measurements in Mediterranean rivers." Journal of Hydrology, Elsevier B.V., 394(1–2), 42–52.

Creutin, J. D., Muste, M., Bradley, A. A., Kim, S. C., and Kruger, A. (2003). "River gauging using PIV techniques: A proof of concept experiment on the Iowa River." Journal of Hydrology, 277(3–4), 182–194.

Dai, A., Qian, T., Trenberth, K. E., and Milliman, J. D. (2009). "Changes in continental freshwater discharge from 1948 to 2004." Journal of Climate, 22(10), 2773–2792.

Detert, M., and Weitbrecht, V. (2015). "A low-cost airborne velocimetry system: Proof of concept." Journal of Hydraulic Research, 53(4), 532–539.

Dombroski, D. E., and Crimaldi, J. P. (2007). "The accuracy of acoustic Doppler velocimetry measurements in turbulent boundary layer flows over a smooth bed." Limnology and Oceanography: Methods, 5(1), 23–33.

Farina, G., Alvisi, S., Franchini, M., and Moramarco, T. (2014). "Three methods for estimating the entropy parameter M based on a decreasing number of velocity measurements in a river cross-section." Entropy, 16(5), 2512–2529.

Feloni, E. G., Karpouzos, D. K., and Baltas, E. A. (2018). "Optimal hydrometeorological station network design using GIS techniques and multicriteria decision analysis." Journal of Hazardous, Toxic, and Radioactive Waste, 22(3), 1–8.

Fischler, M. A., and Bolles, R. C. (1981). "Random sample consensus." Communications of the ACM, 24(6), 381–395.

Fuh, C.-S., and Maragos, P. (1991). "Motion displacement estimation using an affine model for image matching." Optical Engineering, 30(7), 881–887.

Götzinger, J., and Bárdossy, A. (2008). "Generic error model for calibration and uncertainty estimation of hydrological models." Water Resources Research, 44(12), 1–18.

Hamilton, S. (2012). "The 5 essential elements of a hydrological monitoring programme." Bulletin - World Meteorological Organization, World Meteorological Organization (WMO), Geneva.

Hassaballah, M., Alshazly, H. A., and Ali, A. A. (2019). "Analysis and Evaluation of Keypoint Descriptors for Image Matching." ResearchGate, Studies in Computational Intelligence, M. Hassaballah and K. M. Hosny, eds., Springer International Publishing, Cham, 113–140.

Jodeau, M., Hauet, A., Paquier, A., Le Coz, J., and Dramais, G. (2008). "Application and evaluation of LS-PIV technique for the monitoring of river surface velocities in high flow conditions." Flow Measurement and Instrumentation, 19(2), 117–127.

Kochilakis, G., Poursanidis, D., Chrysoulakis, N., Varella, V., Kotroni, V., Eftychidis, G., Lagouvardos, K., Papathanasiou, C., Karavokyros, G., Aivazoglou, M., Makropoulos, C., and Mimikou, M. (2016). "FLIRE DSS: A web tool for the management of floods and wildfires in urban and periurban areas." Open Geosciences, 8(1), 711–727.

Kossieris, P., Makropoulos, C., Onof, C., and Koutsoyiannis, D. (2018). "A rainfall disaggregation scheme for sub-hourly time scales: Coupling a Bartlett-Lewis based model with adjusting procedures." Journal of Hydrology, Elsevier B.V., 556, 980–992.

Moraitis, G., and Baltas, E. (2019). "Methodological approach for GCP independent LSPIV measurement from moving drone: A proof of concept." 14th Conference of Hellenic Hydrotechnical Association, Volos, Greece, 652–665.

Morales, R., Ettema, R., and Barkdoll, B. (2008). "Large-Scale Flume Tests of Riprap-Apron Performance at a Bridge Abutment on a Floodplain." Journal of Hydraulic Engineering, 134(6), 800–809.

Moramarco, T., Barbetta, S., and Tarpanelli, A. (2017). "From surface flow velocity measurements to discharge assessment by the entropy theory." Water (Switzerland), 9(2).

Mueller, D. S., and Wagner, C. R. (2009). "Measuring discharge with acoustic Doppler current profilers from a moving boat." U. S. Geological Survey Techniques and Methods 3–A22, U.S. Geological Survey (USGS), (December), 72.

Muste, M., Hauet, A., Fujita, I., Legout, C., and Ho, H. C. (2014). "Capabilities of large-scale particle image velocimetry to characterize shallow free-surface flows." Advances in Water Resources, 70, 160–171.

Petersen-Øverleir, A. (2006). "Modelling stage-discharge relationships affected by hysteresis using the Jones formula and nonlinear regression." Hydrological Sciences Journal, 51(3), 365–388.

Rosten, E., and Drummond, T. (2005). "Fusing points and lines for high performance tracking." Tenth IEEE International Conference on Computer Vision (ICCV'05) Volume 1, 1508-1515 Vol. 2.

Sappa, G., Ferranti, F., and Pecchia, G. M. (2015). "Validation Of Salt Dilution Method For Discharge Measurements In The Upper Valley Of Aniene River (Central Italy)." Recent Advances in Environment, Ecosystems and Development, 42–48.

Sichangi, A. W., Wang, L., Yang, K., Chen, D., Wang, Z., Li, X., Zhou, J., Liu, W., and Kuria, D. (2016). "Estimating continental river basin discharges using multiple remote sensing data sets." Remote Sensing of Environment, The Authors, 179, 36–53.

Tauro, F., Olivieri, G., Petroselli, A., Porfiri, M., and Grimaldi, S. (2016a). "Flow monitoring with a camera: a case study on a flood event in the Tiber River." Environmental Monitoring and Assessment, 188(2), 118.

Tauro, F., Porfiri, M., and Grimaldi, S. (2016b). "Surface flow measurements from drones." Journal of Hydrology, Elsevier B.V., 540, 240–245.

Torr, P. H. S. (2002). "Bayesian model estimation and selection for epipolar geometry and generic manifold fitting." International Journal of Computer Vision, 50(1), 35–61.

UNDRR. (2015). The Human Cost of Weather-Related Disasters 1995-2015. Geneva, Switzerland.

UNDRR. (2019). Global Assessment Report on Disaster Risk Reduction. Geneva, Switzerland.

Voulgaris, G., and Trowbridge, J. H. (1998). "Evaluation of the Acoustic Doppler Velocimeter (ADV) for Turbulence Measurements*." Journal of Atmospheric and Oceanic Technology, 15(1), 272–289.

Willert, C. E., and Gharib, M. (1991). "Digital particle image velocimetry." Experiments in Fluids, 10(4), 181–193.

WMO. (2008). Guide to Hydrological Practices. Volume I: Hydrology–From Measurement to Hydrological Information. WMO-No. 168, World Meteorological Organization, Geneva,Switzerland.

Zhang, Z. (2000). "A flexible new technique for camera calibration." IEEE Transactions on Pattern Analysis and Machine Intelligence, 22(11), 1330–1334.